Molecular Distortion of *trans*-Stilbene and the Raman Intensity of the In-Phase CH Out-of-Plane Wag of the Central CH═CH Group†

Kazuhiko Furuya, Kouji Kawato, and Hiroshi Yokoyama

Ashigara Research Laboratories, Fuji Photo Film Company Ltd., 210 Nakanuma, Minami-Ashigara, Kanagawa 250-0193, Japan

Akira Sakamoto and Mitsuo Tasumi*

Department of Chemistry, Faculty of Science, Saitama University, Saitama 338-8570, Japan

Received: January 8, 2003; In Final Form: May 7, 2003

A long-standing issue, i.e., whether the molecule of *trans*-stilbene is distorted around the central C═C bond and/or the C−phenyl bond in solution, is examined by performing density functional calculations of the Raman intensity of the in-phase CH out-of-plane wag of the central CH═CH group. Dependencies of the Raman intensity of the said mode upon the torsional angles around the central C═C and C−phenyl bonds are calculated. Not only the normal species of *trans*-stilbene but also two isotope-labeled species, $C_6H_5{}^{13}CH={}^{13}CHC_6H_5$ and $C_6H_5CD=CDC_6H_5$, are treated. Comparisons of the calculated results with the observed spectra show that the *trans*-stilbene molecule is distorted in solution. The ranges of distortion around the central C═C and C−phenyl bonds are estimated to be 2.5−4.0° and 8.0−12.0°, respectively, from the planar arrangement around the respective bonds.

1. Introduction

Whether a π-conjugated organic molecule is planar or nonplanar is an interesting question in itself in relation to the balance of forces determining its geometrical structure at equilibrium. This problem may have more global importance in view of the fact that biologically important polyene chromophores such as retinal in rhodopsin and bacteriorhodopsin as well as carotenoids in photosynthetic systems are distorted from planarity in biologically active conditions.[1,2] The present paper reports a vibrational study of nonplanarity of a basic organic molecule, *trans*-stilbene, in solution.

In 1976, Edelson and Bree[3] reported that, in the Raman spectra of *trans*-stilbene (tSB) in a CCl_4 solution and in the melt, a band at 960 cm^{-1} was dramatically intensified in comparison with the extremely weak intensity of the same band in the spectrum of solid tSB. They pointed out that this Raman band coincided in wavenumber position with a very strong infrared band of tSB. The infrared band at 959 cm^{-1} is undoubtedly assignable[4] to a mode consisting predominantly of the in-phase CH out-of-plane wag of the central CH═CH group (hereafter called the in-phase ethylenic CH wag) as depicted in Figure 1 (adapted from our recent paper[4]), where the two hydrogen atoms in the central CH═CH group move in phase out of the CH═CH plane. If the tSB molecule assumes a centrosymmetric planar structure (C_{2h} symmetry), the in-phase ethylenic CH wag belonging to the a_u species should be infrared-active but Raman-inactive.

On the basis of the above findings and considerations, Edelson and Bree concluded as follows. The enhancement of the Raman intensity of the 960 cm^{-1} band in the liquid phase is due to the distortion of the tSB molecule from the planar structure, whereas the tSB molecule is essentially planar in the solid state in accord with the results of X-ray analyses.[5−8] Bree and Edelson furthered their view in a later study[9] on the low-frequency Raman spectra of tSB in the solid state.

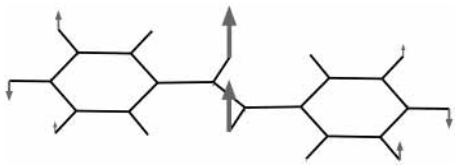

Figure 1. Vibrational mode of the in-phase ethylenic CH out-of-plane wag (ν_{27}).

The following questions arise as to the above conclusion:

(1) Which distortions are more responsible for the Raman intensity of the 960 cm^{-1} band: the central C═C bond or the C−phenyl bond (hereafter abbreviated as C−Ph)? From the descriptions in refs 3 and 9, Edelson and Bree were not clear at this point, although a stronger possibility of the distortion around the C−Ph bond was probably suggested.

(2) What is the degree of molecular distortion?

(3) Is it reasonable to consider that the molecular distortion selectively enhances the Raman intensity of the in-phase ethylenic CH wag and gives little effects on the other modes?

The present paper aims to answer these questions by performing density functional calculations of the Raman intensities for distorted model structures of tSB. Some confirmatory measurements of the Raman and infrared spectra of tSB and its isotopically substituted analogues in solution and in the solid state are also carried out for this aim.

2. Computational and Experimental Procedures

Molecular structural parameters, vibrational wavenumbers, vibrational modes, Raman activities, and other properties were

† Part of the special issue "A. C. Albrecht Memorial Issue".

* Corresponding author: fax +81-48-858-9473; e-mail tasumi@chem.saitama-u.ac.jp.

10.1021/jp0300039 CCC: $25.00
Published on Web 07/12/2003

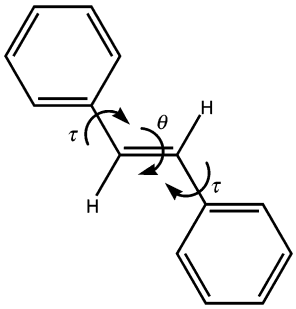

Figure 2. Torsional angles θ and τ.

calculated for the tSB molecule by varying the torsional angle around the central C═C bond (θ) and that around the C−Ph bond (τ) (see Figure 2), which are defined in more detail in the next paragraph. The τ angles around the two C−Ph bonds were changed simultaneously to make the molecule retain C_2 symmetry.

The angle θ is defined as the torsional angle around the central C═C bond in the H−C═C−H linkage in a way consistent with the IUPAC Recommendations on the Definition and Symbolism of Molecular Force Constants.[10] Similarly, the angle τ is defined around the C−Ph bond in the C═C−C−C linkage (the last C atom being cis to the first C atom in the planar structure). Thus, in the case of the planar structure, θ and τ are equal to 180° and 0°, respectively. Changes in θ and τ from the planar structure are expressed as $\Delta\theta$ and $\Delta\tau$, which are positive for a clockwise torsion around the respective bond and negative for an anticlockwise torsion.

The angles $\Delta\theta$ and $\Delta\tau$ were first independently varied from 0° to 20° at intervals of 4°. Optimization of structural parameters except for θ and τ was carried out for each model structure having a set of prefixed values of θ and τ. Spectral simulations were performed for six model structures with $\Delta\theta$ in the range of 2.5−4.0° and $\Delta\tau$ in the ranges of 4.0−12.0° and −(4.0−12.0°).

Density functional calculations were performed by using the B3LYP functional[11,12] in combination with the 6-311+G** basis set. The Gaussian 98 revision A.9 program package[13] was used at a network parallel execution mode with Linda (embedded in Gaussian 98) on a computer system HPC Alpha 21264 (500 MHz × 4 CPU).

The wavenumbers of the normal vibrations calculated by density functional theory were multiplied by a single scaling factor of 0.9785[4] to have a good fit between the observed and scaled wavenumbers. By this uniform scaling, the differences between the observed and corresponding calculated wavenumbers were made to be within 10 cm^{-1}. In the band assignments, the calculated Raman and infrared intensities were also fully taken into account.[4]

Two kinds of isotope-labeled species, $C_6H_5{}^{13}CH{=}{}^{13}CHC_6H_5$ (tSB-$^{13}C_2$) and $C_6H_5CD{=}CDC_6H_5$ (tSB-d_2), which were obtained some years ago and kept by the Hamaguchi group at the University of Tokyo, were used. The Raman spectrum of tSB-$^{13}C_2$ coincided with that reported by Gustafson et al.[14] The sample of tSB-d_2 was synthesized according to the method described by Hamaguchi et al.[15] The Raman and infrared spectra of tSB-d_2 were essentially the same as those reported by Meić and Güsten.[16]

For spectral measurements in solution, benzene and *n*-hexane were used as solvents. In the Raman measurements, C_6D_6 was used as solvent instead of normal benzene, because the very strong Raman band of normal benzene at 993 cm^{-1} interfered with accurate measurements of the most informative spectral region of tSB. Concentration in C_6D_6 solution was 0.5 mol dm^{-3}. When *n*-hexane was the solvent, a saturated solution (concentration less than 0.05 mol dm^{-3}) was used.

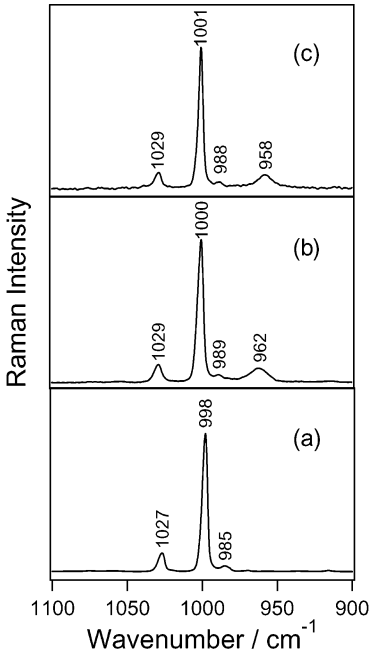

Figure 3. Raman spectrum of tSB in the 1100−900 cm^{-1} region: (a) powder; (b) C_6D_6 solution; (c) *n*-hexane solution.

Raman spectral measurements were performed with a Bruker RFS 100 Fourier transform Raman spectrometer by using Nd:YAG 1064-nm light for Raman measurements. Infrared spectra were recorded on a Bio-Rad FTS-40 Fourier transform infrared spectrophotometer. Both Raman and infrared measurements for tSB were performed at 1 cm^{-1} resolution. Interferograms from 4000, 8000, and 1024 scans were averaged in the Raman measurements of tSB in C_6D_6, *n*-hexane, and the solid state (powder), respectively. Measurements for tSB-$^{13}C_2$ were made under similar conditions. The Raman spectrum of tSB-d_2 in C_6D_6 solution was obtained at 4 cm^{-1} resolution by averaging 16 000 scans, because the Raman band due to the in-phase CD out-of-plane wag is very weak in intensity.

3. Results and Discussion

In this section, mention is frequently made of the band assignments of tSB, which were discussed in detail in ref 4.

A. Confirmatory Measurements of the Raman Spectra of tSB in Deuterated Benzene and *n*-Hexane Solutions. To confirm that the enhancement of the intensity of the Raman band at 960 cm^{-1} of tSB is commonly observed in solution, the Raman spectra of tSB were measured in deuterated benzene (C_6D_6) and *n*-hexane solutions. The spectra in the 1100−900 cm^{-1} region, where the most interesting results are observed, are shown in Figure 3, together with the spectrum obtained from a powder sample. Clearly, a weak band is observed at 962 cm^{-1} in C_6D_6 solution and at 958 cm^{-1} in *n*-hexane solution, whereas no band is observed at about 960 cm^{-1} in the powder spectrum. In C_6D_6 solution, two bands, a weak one at 1029 cm^{-1} and a strong one at 1000 cm^{-1}, are observed, which are assigned,[4] respectively, to ν_{19} and ν_{20} in the a_g species. Another very weak band is observed at 989 cm^{-1} in C_6D_6 solution, which is more clearly seen at 985 cm^{-1} in the powder spectrum. This band may be assigned[4] to ν_{38} in the b_g species.

The infrared spectra of tSB were also measured in benzene and *n*-hexane solutions. A strong infrared band is observed at

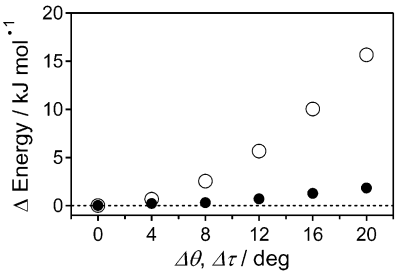

Figure 4. $\Delta\theta$ and $\Delta\tau$ dependencies of the total energy of planar and distorted tSB. ΔEnergy refers to energy increase from the planar structure. ○ and ● show, respectively, the $\Delta\theta$ and $\Delta\tau$ dependencies.

962 cm^{-1} in benzene solution, and it shifts to 959 cm^{-1} in *n*-hexane solution. The 3 cm^{-1} downshift on going from benzene solution to *n*-hexane solution parallels the 4 cm^{-1} downshift observed in the Raman measurements. (The difference of 1 cm^{-1} between the peak wavenumbers of the Raman and infrared bands observed in *n*-hexane solution is allowable under the present experimental conditions.) These results convincingly show that the Raman band observed in solution at about 960 cm^{-1} has an origin common to the strong infrared band observed at the same wavenumber within experimental error. This strong infrared band is undoubtedly assignable[4] to ν_{27} in a_u, which primarily consists of the in-phase ethylenic CH wag.

The above observations support Edelson and Bree's assertion that the weak Raman band observed in solution at about 960 cm^{-1} arises from the in-phase ethylenic CH wag, which should be Raman-inactive if the tSB molecule is planar.

B. Dependence of the Total Energy on $\Delta\theta$ and $\Delta\tau$. The molecular total energy of tSB was calculated by independently changing $\Delta\theta$ and $\Delta\tau$ from 0° to 20° at 4° intervals. Molecular geometry at each set of the prefixed values of θ and τ was optimized, and these are called model structures. Increase in the energy of each model structure from that of the planar structure, ΔEnergy, is plotted in Figure 4. It is noted that, for an amount of increase in energy, the value of $\Delta\theta$ giving rise to this increase is approximately $^1/_3$ the value of $\Delta\tau$ doing the same. For example, $\Delta\theta = 2.5°$ gives a comparable increase in energy as $\Delta\tau = 8.0°$, and $\Delta\theta = 4.0°$ does the same as $\Delta\tau = 12.0°$. This result is reasonable, since (1) $\Delta\theta$ refers to the torsion around the central C═C bond, which definitely has a double-bond character,[4,7] and (2) $\Delta\tau$ refers to the torsion around the C−Ph bond, which may be regarded as a single bond although its length is slightly shorter than the length of a typical C−C single bond.[4,7]

The results obtained above seem to have the following implications. In the distorted molecule, there is no reason ΔEnergy is localized in the torsional degree of freedom around a particular bond. In other words, the total ΔEnergy should be equally borne by the torsional displacements around the central C═C and the C−Ph bonds. Then, it seems most reasonable to consider that the value of $\Delta\theta$ should be about $^1/_3$ that of $\Delta\tau$ in the distorted molecule of tSB, if it really exists.

The fully optimized geometry of the tSB molecule is planar. Then, a question may arise as to the legitimacy of performing normal coordinate calculations for model structures that are more or less deviated from the true potential minimum. However, such an approach may be permitted for the purpose of the present study, since the in-phase ethylenic CH wag and other modes to be discussed in this paper are orthogonal to the torsional modes around the central C═C bond and the C−Ph bond, and their frequencies are much higher than the torsional frequencies.

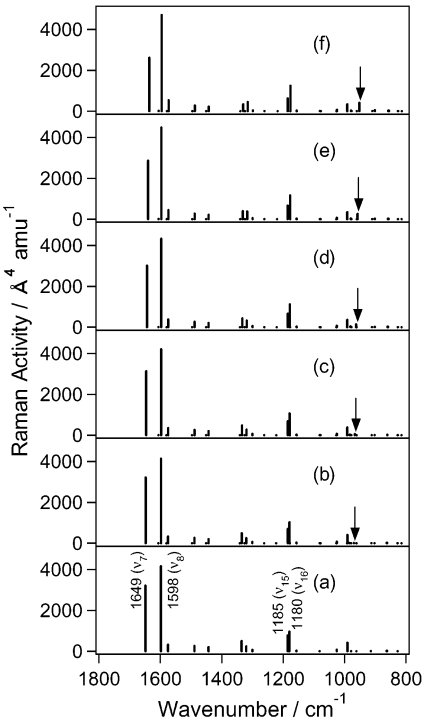

Figure 5. $\Delta\theta$ dependency of the calculated Raman spectrum of tSB in the 1800−800 cm^{-1} region. $\Delta\theta$ = (a) 0°, (b) 4°, (c) 8°, (d) 12°, (e) 16°, and (f) 20°. $\tau = 0°$ in all cases. Arrow indicates the ν_{27} band.

C. Dependence of the Raman Intensity of the In-Phase Ethylenic CH Wag on $\Delta\theta$. Calculations of the Raman spectra of model structures of tSB with $\Delta\theta = 0-20°$ changing at 4° intervals and $\tau = 0°$ in all cases were performed. The calculated results in the wavenumber region of 1800−800 cm^{-1} are shown as stick spectra in Figure 5. It is seen in this figure that the departure of $\Delta\theta$ from 0° not only causes some changes in wavenumber position and intensity for many bands existing at $\Delta\theta = 0°$ but also gives rise to a number of very weak bands nonexistent at $\Delta\theta = 0°$. Among the bands in the latter group, only the band calculated at 967 cm^{-1} (indicated with arrow) becomes definitely stronger with increasing $\Delta\theta$. This band is due to the in-phase ethylenic CH wag (ν_{27}).

In Figure 6, the 1100−900 cm^{-1} region of Figure 5 is enlarged. Clearly, the ν_{27} band (indicated with arrow) steadily grows and shifts to lower wavenumbers with increasing $\Delta\theta$. The band calculated at 991 cm^{-1} (ν_{20} in a_g), assigned[4] to the strong Raman band at 1000 cm^{-1} (Figure 3b), slightly decreases in intensity with increasing $\Delta\theta$. The calculated activities of these two modes, ν_{20} and ν_{27}, are plotted in Figure 7. The results in Figures 6 and 7 show that a marked increase in the intensity of ν_{27} occurs with $\Delta\theta$ changing from 0° to 20°. The band calculated at 1025 cm^{-1} (ν_{19} in a_g), assigned[4] to a weak Raman band at 1029 cm^{-1} (Figure 3b), does not show a definite change in intensity with $\Delta\theta$ changing from 0° to 20°. Two very weak bands are calculated at 985 and 979 cm^{-1} (Figure 6a,b). The origin of the 985 cm^{-1} band (ν_{26} in a_u) will be discussed later. The 979 cm^{-1} band, which exists in the spectrum at $\Delta\theta = 0°$ (Figure 6a), corresponds to ν_{38} in b_g mentioned in section A. Another even weaker band, which is due to ν_{39} in b_g,[4] is calculated at 962 cm^{-1} (Figure 6a). Since this band shows no change in either intensity or wavenumber position with increasing $\Delta\theta$ (Figure 6), it may be disregarded in the present discussion.

D. Dependence of the Raman Intensity of the In-Phase Ethylenic CH Wag on $\Delta\tau$. In parallel with the case described

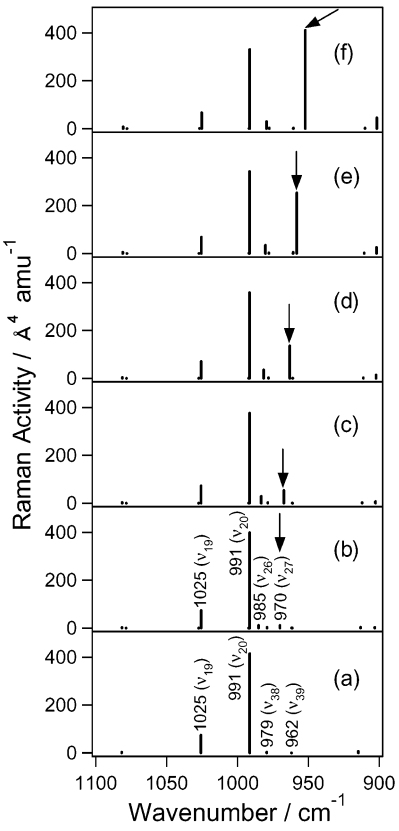

Figure 6. $\Delta\theta$ dependency of the calculated Raman spectrum of tSB enlarged in the 1100−900 cm^{-1} region. $\Delta\theta$ = (a) 0°, (b) 4°, (c) 8°, (d) 12°, (e) 16°, and (f) 20°. τ = 0° in all cases. Arrow indicates the ν_{27} band.

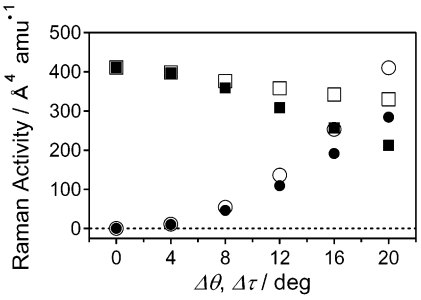

Figure 7. $\Delta\theta$ and $\Delta\tau$ dependencies of the Raman activities of ν_{20} and ν_{27}. Open symbols show the $\Delta\theta$ dependency, and solid symbols show the $\Delta\tau$ dependency. Squares represent ν_{20}; circles represent ν_{27}.

in section C, the Raman spectra of model structures with $\Delta\tau$ = 0−20° changing at 4° intervals and θ = 180° in all cases were calculated. The results in the 1800−800 cm^{-1} region are shown in Figure 8. The departure of $\Delta\tau$ from 0° also gives rise to the Raman intensity of ν_{27} (indicated with arrow). This result is similar to the case described in section C for model structures with changing $\Delta\theta$. However, the Raman intensities of some bands depend on $\Delta\tau$ in a way different from their dependencies on $\Delta\theta$. For example, the calculated intensities of the bands at 1649 (ν_7 in a_g) and 1598 (ν_8 in a_g) cm^{-1}, assigned,[4] respectively, to the very strong Raman bands at 1639 and 1600 cm^{-1}, depend differently on $\Delta\theta$ and $\Delta\tau$; in Figure 5, the intensity of ν_7 gradually decreases with increasing $\Delta\theta$ and that of ν_8 gradually increases, whereas in Figure 8, the intensity of ν_7 slightly decreases with increasing $\Delta\tau$ and that of ν_8 also decreases significantly. A similar trend is seen for the two bands calculated at 1185 (ν_{15}) and 1180 (ν_{16}) cm^{-1}, assigned,[4] respectively, to

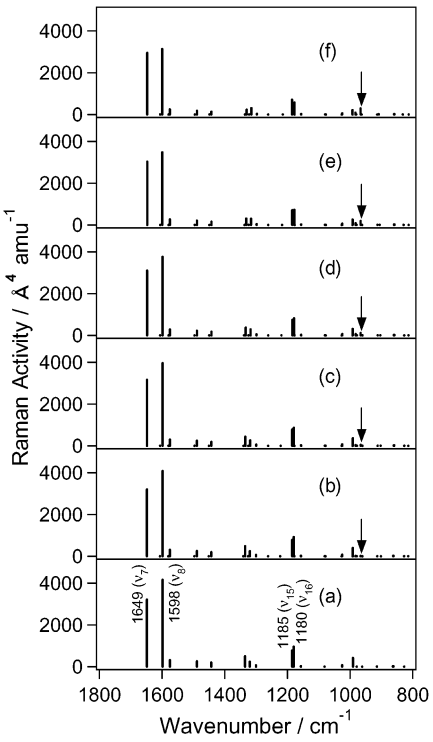

Figure 8. $\Delta\tau$ dependency of the calculated Raman spectrum of tSB in the 1800−800 cm^{-1} region. $\Delta\tau$ = (a) 0°, (b) 4°, (c) 8°, (d) 12°, (e) 16°, and (f) 20°. θ = 180° in all cases. Arrow indicates the ν_{27} band.

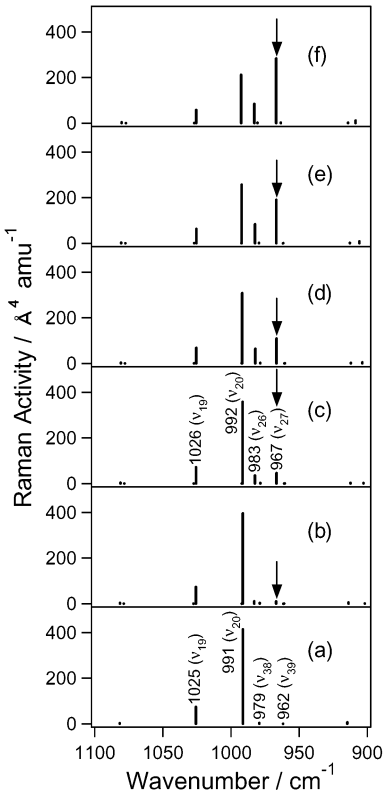

Figure 9. $\Delta\tau$ dependency of the calculated Raman spectrum of tSB enlarged in the 1100−900 cm^{-1} region. $\Delta\tau$ = (a) 0°, (b) 4°, (c) 8°, (d) 12°, (e) 16°, and (f) 20°. θ = 180° in all cases. Arrow indicates the ν_{27} band.

the strong Raman band at 1194 cm^{-1} and the weak Raman band at 1183 cm^{-1}.

In Figure 9, the 1100−900 cm^{-1} region of Figure 8 is enlarged. The enhancement of the intensity of the ν_{27} band with

increasing $\Delta\tau$ is clear, but the degree of the intensity enhancement of ν_{27} with increasing $\Delta\tau$ is smaller than that with increasing $\Delta\theta$, as shown in Figure 7. On the other hand, the intensity decrease of ν_{20} with increasing $\Delta\tau$ in Figure 9 is more rapid than that with increasing $\Delta\theta$, as shown in Figure 7.

It is noted in Figure 9 that another band is calculated at 983 cm^{-1} with a Raman intensity comparable with that of ν_{27} (Figure 9c). The intensity of this band is also enhanced with increasing $\Delta\tau$ but not as markedly as that of the ν_{27} band. (Actually, a band corresponding to this band exists in Figure 6 also, but its intensity does not increase with increasing $\Delta\theta$.) According to the results of the present calculations, the 983 cm^{-1} band is due to ν_{26} in a_u,[4] which is a mode assignable to a CH out-of-plane wag of the phenyl ring (a ring CH wag for short) but has a considerable contribution of the in-phase ethylenic CH wag.[4] Similarly, as seen in Figure 1, ν_{27} may be called the in-phase ethylenic CH wag but has a contribution of the ring CH wag as well.

In other words, the in-phase ethylenic CH wag and the ring CH wag tend to mix in ν_{26} and ν_{27}. The in-phase ethylenic wag must be the mode giving rise to the Raman intensity when the tSB molecule is distorted, but the ring CH wag is not expected to behave in a similar manner. Therefore, it is most likely that the degree of the mode mixing between the two wags in ν_{26} is overestimated in the present calculations, because, as described in section A, only the band observed at about 960 cm^{-1} (962 cm^{-1} in benzene solution and 958 cm^{-1} in *n*-hexane solution) definitely acquires its Raman intensity on going from solid to solution. To examine this point in more detail, calculations and Raman measurements were extended to two kinds of isotope-labeled species, tSB-$^{13}C_2$ and tSB-d_2. Similar attempts on $C_6D_5CH{=}CHC_6D_5$ were not fruitful, because a strong Raman band due to the C_6D_5 group was observed in close proximity to the expected position of the in-phase ethylenic CH wag.

E. Raman Measurements and Calculations for tSB-$^{13}C_2$. The 1100−900 cm^{-1} region of the Raman spectrum of tSB-$^{13}C_2$ observed in benzene solution is almost the same as that of the normal species in Figure 3b, except that the 962 cm^{-1} band of the normal species shifts to 958 cm^{-1} in the spectrum of tSB-$^{13}C_2$. The ν_{26} and ν_{27} bands are calculated at 983 and 965 cm^{-1} for the planar structure of tSB-$^{13}C_2$. This means that only the ν_{27} band shifts by 2 cm^{-1} upon ^{13}C substitution in the calculated results, in comparison with the observed shift of 4 cm^{-1} mentioned above. The results of calculation show that this small shift, which causes a larger separation between ν_{26} and ν_{27} of tSB-$^{13}C_2$, is clearly accompanied by a decrease in the extent of mode mixing between the in-phase ethylenic CH wag and the ring CH wag in ν_{26} and ν_{27} of tSB-$^{13}C_2$; ν_{26} has a smaller contribution of the in-phase ethylenic CH wag than in the case of the normal species, and ν_{27} has a larger contribution of the same. The results of calculation for distorted model structures of tSB-$^{13}C_2$ show that the Raman intensity of ν_{26} is less enhanced with molecular distortion than in the case of the normal species, reflecting the decreased mixing of the in-phase ethylenic CH wag.

The results described above for tSB-$^{13}C_2$ are consistent with the inference that (1) ν_{26} of the normal species would actually have a smaller contribution of the in-phase ethylenic CH wag than indicated in the present calculations, and accordingly little enhancement of the Raman intensity would occur for ν_{26} with molecular distortion, and (2) ν_{27} of the normal species would consist predominantly of the in-phase ethylenic CH wag giving rise to the enhanced Raman intensity for ν_{27} with molecular distortion.

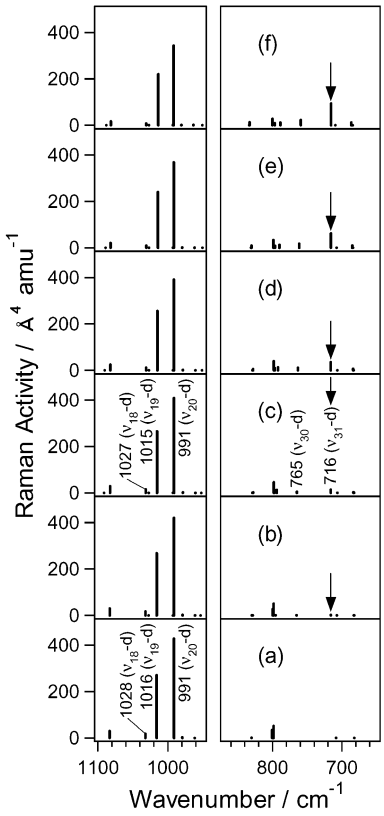

Figure 10. $\Delta\tau$ dependency of the calculated Raman spectrum of tSB-d_2 in the 1100−650 cm^{-1} region. $\Delta\tau$ = (a) 0°, (b) 4°, (c) 8°, (d) 12°, (e) 16°, and (f) 20°. θ = 180° in all cases. Arrow indicates the ν_{31}-*d* band.

F. Raman Measurements and Calculations for tSB-d_2. Calculations for distorted model structures of tSB-d_2 show that ν_{31}-*d*, which corresponds to ν_{27} of the normal species and consists almost solely of the in-phase ethylenic CD wag, is located at 716 cm^{-1}. In fact, a very weak Raman band is observed at 714 cm^{-1} in C_6D_6 solution (observed spectrum to be shown later). An infrared band corresponding to this Raman band is observed at 715 cm^{-1} with an intensity considerably decreased from the infrared intensity of the 962 cm^{-1} band of the normal species. In the Raman spectrum of powder tSB-d_2, the 714 cm^{-1} band is not observed at all. This indicates that the 714 cm^{-1} band is not due to an impurity in the sample. The Raman intensity of ν_{31}-*d* calculated for distorted model structures of tSB-d_2 is enhanced with increasing $\Delta\theta$ or $\Delta\tau$, as shown in Figure 10 for the case of $\Delta\tau$ dependency. These results fully confirm the expectation that the tSB-d_2 molecule is planar in the solid state but distorted in C_6D_6 solution.

A noticeable feature in the Raman spectrum of tSB-d_2 is the existence of another band (ν_{30}-*d*) calculated at 767 cm^{-1} for the planar structure (765 cm^{-1} in Figure 10c). As seen in Figure 10, the Raman intensity of this ν_{30}-*d* band is also enhanced with increasing $\Delta\tau$, although the extent of enhancement is smaller than that for ν_{31}-*d*. Examination of the vibrational mode of ν_{30}-*d* indicates that, for the planar structure, it is primarily a ring CH wag similar to ν_{31} of the normal species[4] with a very small contribution of the in-phase ethylenic CD wag, but the contribution of the in-phase ethylenic CD wag becomes larger with increasing $\Delta\tau$. This increased mixing of the in-phase ethylenic CD wag in ν_{30}-*d* with increasing $\Delta\tau$ is probably real, because an extremely weak band seems to exist at 763 cm^{-1} in the Raman spectrum of tSB-d_2 in C_6D_6 solution, but no corresponding band exists in the powder spectrum. The situation described

here is similar to that mentioned in section D for ν_{26} of the normal species. The difference between ν_{30}-*d* of tSB-d_2 and ν_{26} of the normal species is that the present calculations give rise to an overestimated mode mixing in ν_{26} of the normal species, as well as the too-small calculated separation between ν_{26} and ν_{27} of the normal species (16 cm^{-1} for the planar structure), but estimate the mode mixing in ν_{30}-*d* of tSB-d_2 more appropriately. In the latter, the calculated separation between ν_{30}-*d* and ν_{31}-*d* of tSB-d_2 is larger (51 cm^{-1} for the planar structure).

In Figure 10, five very weak bands are calculated in the region of 850−770 cm^{-1} as $\Delta\tau$ departs from zero. Their intensities change with $\Delta\tau$, but it is difficult to discuss the molecular distortion based on these results, since three bands are expected to exist for the planar structure and they suffice to account for the Raman spectrum observed in this region.

G. Estimation of $\Delta\theta$ and $\Delta\tau$ in the Distorted Structure in C_6D_6 Solution by Simulations of the Raman Spectra in the Regions of the In-Phase Ethylenic CH and CD Wags. From the fact that the spectra observed in C_6D_6 solution and in *n*-hexane solution are essentially similar (Figure 3b,c), it is likely that the tSB molecule in these solutions is distorted to almost the same extent. For estimating $\Delta\theta$ and $\Delta\tau$ in the distorted structure, simulations of the Raman spectra of tSB and tSB-d_2 observed in C_6D_6 solution are performed by fitting appropriate combinations of Gaussian and Lorentzian band shapes to the observed bands, so that differences in the shapes and widths of the observed bands are taken into account. (Such differences in band shapes may be an interesting subject of study but will not be discussed in this paper.)

Basic assumptions adopted in these simulations are that (1) Raman intensities calculated by density functional theory are useful for the present simulation, even if some of them have significant deviations from the observed, and (2) as described in section B, the value of θ should be approximately $^1/_3$ that of τ in the distorted structure. Under these assumptions and by comparing the observed spectrum in Figure 3b with the calculated stick spectra in Figures 6 and 9, the possible ranges of $\Delta\theta$ and $\Delta\tau$ are estimated, respectively, to be 2.5−4.0° and 8.0−12.0°. In the first place, spectral simulations are performed for the following two sets of $\Delta\theta$ and $\Delta\tau$: (2.5°, 8.0°) and (4.0°, 12.0°). Stick Raman spectra for the distorted model structures with these two sets are calculated in the same way as described earlier. The results of simulations indicate that the observed Raman spectrum in C_6D_6 in the 1100−900 cm^{-1} region is halfway between the simulated spectra for these two sets. Then, simulations are performed for an intermediate set of $\Delta\theta$ and $\Delta\tau$ (3.0°, 9.0°). The simulated spectrum for this set is shown in Figure 11, together with the observed spectrum.

In the simulations, the observed three bands at 1029, 1000, and 962 cm^{-1} are simulated by the ν_{19}, ν_{20}, and ν_{27} bands at 1025, 992, and 969 cm^{-1}, respectively, as shown in Figure 11. The ν_{38} band observed very weakly at 989 cm^{-1} is not included in this spectral simulation, since this band is not significant for the purpose of the present discussion. The ν_{26} band calculated at 982 cm^{-1} is not included either, because, as described in detail in section D, the calculated Raman intensity of this ν_{26} band is undoubtedly overestimated. The Gaussian/Lorentzian ratios optimized for the ν_{19}, ν_{20}, and ν_{27} bands are 1/0, 7/2, and 7/2 by peak heights, respectively. The full widths at half-maximum for these bands are 6.3, 4.8, and 15.0 cm^{-1}, respectively.

The observed spectrum in Figure 11a is compared with the results of simulation in Figure 11b,c for $\Delta\theta = 3.0°$ and $\Delta\tau = 9.0°$. The simulated spectrum in Figure 11c is synthesized from the simulated bands in Figure 11b. The peak height of the ν_{20} band in Figure 11c is made equal to the height of the observed band at 1000 cm^{-1} in Figure 11a. In Figure 11b, the calculated stick spectra including the ν_{26} band at 982 cm^{-1} (marked with an asterisk) are shown, where the height of the ν_{20} stick band is made equal to that of the simulated ν_{20} band.

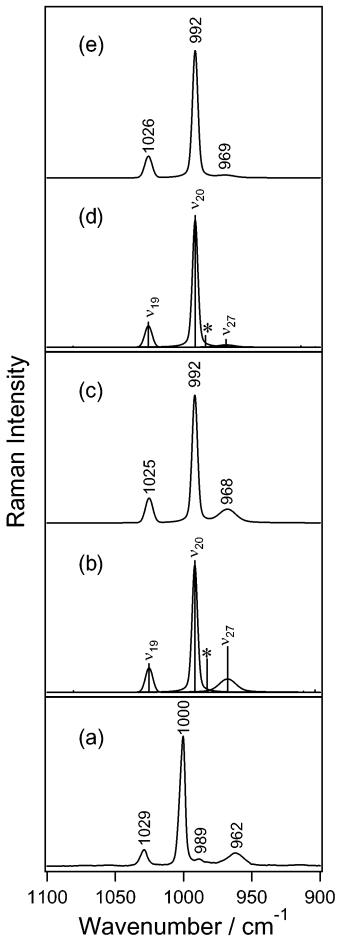

Figure 11. Simulations of the Raman spectrum of tSB in the 1100−900 cm^{-1} region. (a) observed; (b, c) simulated with $\Delta\theta = 3°$ and $\Delta\tau = 9°$; (d, e) simulated with $\Delta\theta = 3°$ and $\Delta\tau = -9°$. The asterisked ν_{26} band is not included in the simulation (see text).

The simulated spectrum for $\Delta\theta = 3.0°$ and $\Delta\tau = 9.0°$ in Figure 11c satisfactorily agrees with the observed spectrum in Figure 11a. The degrees of agreement between the simulated spectra for the two initial sets ($\Delta\theta = 2.5°$ and $\Delta\tau = 8.0°$; $\Delta\theta = 4.0°$ and $\Delta\tau = 12.0°$) and the observed spectrum are slightly lower; the intensity of the ν_{27} band is relatively too weak for $\Delta\theta = 2.5°$ and $\Delta\tau = 8.0°$ and too strong for $\Delta\theta = 4.0°$ and $\Delta\tau = 12.0°$. However, differences between the degrees of agreement are small. Therefore, it seems appropriate to state that the distorted structure of tSB in solution is likely to have $\Delta\theta$ in the range of 2.5−4.0° and $\Delta\tau$ in the range of 8.0−12.0°.

So far, combinations of clockwise torsions round the C═C and C−Ph bonds (i.e., sets of positive $\Delta\theta$ and positive $\Delta\tau$ values) were assumed. A question arises as to what happens if a set of a positive $\Delta\theta$ and a negative $\Delta\tau$ is assumed. Spectral simulations are then performed for the following three sets of $\Delta\theta$ and $\Delta\tau$: (2.5°, −8.0°), (3.0°, −9.0°), and (4.0°, −12.0°). Since similar results are obtained for the three sets, the results of simulations for $\Delta\theta = 3.0°$ and $\Delta\tau = -9.0°$ are shown in Figure 11d,e. It is obvious that the intensity of the ν_{27} band at 969 cm^{-1} is too weak in the simulated spectrum in Figure 11e. This means that mutual cancellation occurs between the changes in polarizability derivatives due to a positive $\Delta\theta$ and a negative

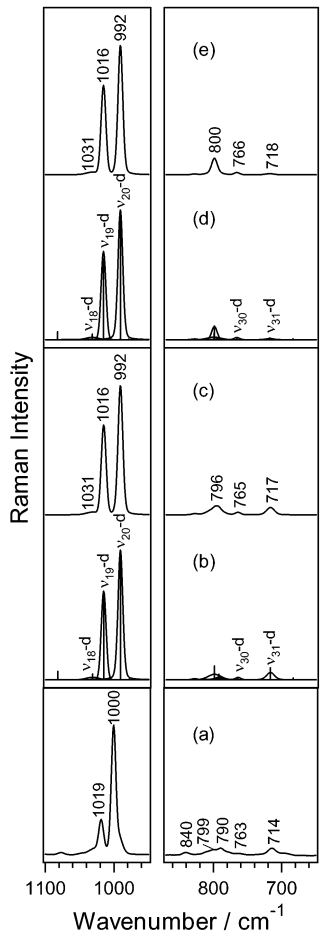

Figure 12. Simulations of the Raman spectrum of tSB-d_2 in the 1100−650 cm^{-1} region. (a) observed; (b, c) simulated with $\Delta\theta = 3°$ and $\Delta\tau = 9°$; (d, e) simulated with $\Delta\theta = 3°$ and $\Delta\tau = -9°$.

$\Delta\tau$. It is likely, therefore, that the distortions around the C=C and C−Ph bonds in the distorted structure of tSB have the same sense.

Spectral simulations are also performed for the Raman spectrum of tSB-d_2 in C_6D_6 solution in the same way as described above. The observed and simulated spectra in the 1100−650 cm^{-1} region are shown in Figure 12. At least eight bands are observed in the spectrum in Figure 12a. The most important band at 714 cm^{-1} arising from the in-phase ethylenic CD wag corresponds to the ν_{31}-d band at 717 cm^{-1} in Figure 12b,c. The strong band observed at 1000 cm^{-1} in Figure 12a, which has exactly the same origin as the 1000 cm^{-1} band of tSB, corresponds to the ν_{20}-d band calculated at 992 cm^{-1} in Figure 12b,c. The medium-intensity band observed at 1019 cm^{-1} in Figure 12a is due to the CD in-plane bend in a_g. In Figure 12b,c, the ν_{19}-d band calculated at 1016 cm^{-1} corresponds to the observed 1019 cm^{-1} band, although the calculated intensity of the ν_{19}-d band is apparently too large. Another weak band exists in the higher-wavenumber tail of the observed 1019 cm^{-1} band. This band (corresponding to the ν_{18}-d band calculated at 1031 cm^{-1} in Figure 12b,c) is due to a ring CH in-plane bend, which bears a close similarity to ν_{19} of the normal species. As described in some detail in section F, the ν_{30}-d band calculated at 766 cm^{-1} (Figure 12b,c) seems to account for an extremely weak band observed around 763 cm^{-1}.

For the present purpose of evaluating the values of θ and τ in the distorted structure, it seems reasonable to compare the intensities of the ν_{20}-d and ν_{31}-d bands in Figure 12b,c with the observed intensities of the corresponding bands in Figure 12a, because the intensity of the ν_{20}-d band is more reliable than that of the ν_{19}-d band. Such comparisons lead to the same conclusion as derived from the above discussion for tSB on the most likely values of $\Delta\theta$ and $\Delta\tau$ in the distorted structure; i.e., they seem to take values intermediate between the set of $\Delta\theta = 2.5°$ and $\Delta\tau = 8.0°$ and the set of $\Delta\theta = 4.0°$ and $\Delta\tau = 12.0°$.

Spectral simulations for tSB-d_2 are also performed for the three sets of positive $\Delta\theta$ and negative $\Delta\tau$ values. The results of simulations for $\Delta\theta = 3.0°$ and $\Delta\tau = -9.0°$ are shown in Figure 12d,e. It is seen in Figure 12e that the ν_{31}-d band at 718 cm^{-1} is too weak, in agreement with the extremely weak intensity of the ν_{27} band at 969 cm^{-1} of tSB in Figure 11e.

H. Possibility of Finding Other Distortion-Sensitive Bands. As mentioned in sections C and D, calculations show that many Raman (and infrared) bands show changes in intensity and/or shifts in wavenumber position upon molecular distortion. However, if the band is expected to exist also for the planar structure, it would be nearly impossible to discern experimentally whether a particular band is distortion-sensitive, unless the intensity change on going from solid to solution is so obvious that it is easily recognized at first glance. Detection of a small change in intensity on going from solid to solution by the technique of taking a difference spectrum is expected to be difficult due to a shift in band position or a change in band shape, which often occurs with the change of states. Only if a band that is forbidden for the planar structure is actually observed would the band be easily recognized as a distortion-sensitive band. Calculations show that such bands should exist but their intensities are expected to be very weak in most cases. Therefore, it would be difficult to find distortion-sensitive bands other than the ν_{27} band, at least in the case of tSB.

I. Why is the Molecule of tSB Distorted in Solution? An important question as to the origin of the 960 cm^{-1} Raman band observed in solution is whether this band is due to the distortion of the molecular structure *at equilibrium* as discussed above or is associated with the existence of thermally excited low-frequency modes. In relation to the latter possibility, Myers et al.[17] discussed the effects of thermally excited low-frequency modes of tSB on the homogeneous and inhomogeneous widths of the electronic absorption and resonance Raman intensities. It should be pointed out, however, that the large-amplitude low-frequency modes do exist not only in tSB in solution but also in tSB in crystal as evidenced by the diffuse X-ray diffraction patterns of crystalline tSB.[8] As described earlier, the 960 cm^{-1} band is practically nonexistent in the Raman spectrum of tSB in the solid state. These experimental results seem to indicate that the molecular structure at equilibrium of tSB is nonplanar in solution, whereas it is planar in the solid state.

Then, why is the molecule of tSB in solution distorted from the planar structure? No simple answer to this question is available at present. Both the present density functional theory calculations and the Hartree−Fock calculations indicate that the optimized geometry of tSB in a vacuum is planar. Solvation, dimerization, clustering, etc., occurring in solution or in the liquid state may account for the stabilization of the system accompanied by molecular distortion, but no evidence for any of such possibilities has been obtained. It would be desirable to perform advanced molecular dynamics calculations for tSB in solutions to obtain an insight into this problem. It is also required to perform quantum chemical calculations of the molecular geometry at levels higher than the present one, to examine the possibility that an isolated tSB molecule has a true potential minimum at a slightly nonplanar structure.

4. Conclusions

(1) The following two points were experimentally confirmed: (a) tSB in solution shows a weak Raman band at about 960 cm^{-1}, which is not observed in the solid state. (b) This band arises from the in-phase ethylenic CH wag, which gives rise to a strong infrared band at the same wavenumber position within experimental error.

(2) Normal coordinate analyses of distorted model structures of tSB based on density functional theory calculations show that the in-phase ethylenic CH wag, which is Raman-inactive for the planar structure, acquires higher Raman intensities with increasing degree of molecular distortion.

(3) The degree of distortion around the ethylenic C═C bond should be $^1/_3$ that around the C−Ph bond, according to the results of density functional theory calculations.

(4) The probable range of distortion around the ethylenic C═C bond is 2.5−4.0° and that around the C−Ph bond is 8.0−12.0° from the planar structure. It is likely that the distortions around the C═C and C−Ph bonds have the same sense.

(5) It is highly possible that the Raman band at about 960 cm^{-1} is practically the only distortion-sensitive band of tSB.

Acknowledgment. We thank Professor Hiro-o Hamaguchi and co-workers for keeping the isotope-labeled samples for a long time and making these samples available for this study.

References and Notes

(1) Mathies, R. A.; Lugtenburg, J. In *Molecular Mechanisms in Visual Transduction*; Stavenga, D. G., DeGrip, W. J., Pugh, E. N., Jr., Eds.; Elsevier Science: Amsterdam, 2000; *Handbook of Biological Physics*, Vol. 3, Chapt. 2, p 55.

(2) Tasumi, M.; Sakamoto, A.; Hieda, T.; Torii, H. In *Handbook of Vibrational Spectroscopy*; Chalmers, J. M., Griffiths, P. R., Eds.; Wiley: New York, 2002; Vol. 3, p 1983.

(3) Edelson, M.; Bree, A. *Chem. Phys. Lett.* **1976**, *41*, 562.

(4) Watanabe, H.; Okamoto, Y.; Furuya, K.; Sakamoto, A.; Tasumi, M. *J. Phys. Chem. A* **2002**, *106*, 3318.

(5) Finder, C. J.; Newton, M. G.; Allinger, N. J. *Acta Crystallogr. B* **1974**, *30*, 411.

(6) Bernstein, J. *Acta Crystallogr. B* **1975**, *31*, 1268.

(7) Bouwstra, J. A.; Schouten, A.; Kroon, J. *Acta Crystallogr. C* **1984**, *40*, 428.

(8) Ogawa, K.; Sano, T.; Yoshimura, S.; Takeuchi, Y.; Toriumi, K. *J. Am. Chem. Soc.* **1991**, *114*, 1041.

(9) Bree, A.; Edelson, M. *Chem. Phys.* **1980**, *51*, 77.

(10) Morino, Y.; Shimanouchi, T. *Pure Appl. Chem.* **1978**, *50*, 1707.

(11) Becke, A. D. *J. Chem. Phys.* **1993**, *98*, 5648.

(12) Lee, C.; Yang, W.; Parr, R. G. *Phys. Rev. B* **1988**, *37*, 785.

(13) Frisch, M. J.; Trucks, G. W.; Schlegel, H. B.; Scuseria, G. E.; Robb, M. A.; Cheeseman, J. R.; Zakrzewski, V. G.; Montgomery, J. A., Jr.; Stratmann, R. E.; Burant, J. C.; Dapprich, S.; Millam, J. M.; Daniels, A. D.; Kudin, K. N.; Strain, M. C.; Farkas, O.; Tomasi, J.; Barone, V.; Cossi, M.; Cammi, R.; Mennucci, B.; Pomelli, C.; Adamo, C.; Clifford, S.; Ochterski, J.; Petersson, G. A.; Ayala, P. Y.; Cui, Q.; Morokuma, K.; Malick, D. K.; Rabuck, A. D.; Raghavachari, K.; Foresman, J. B.; Cioslowski, J.; Ortiz, J. V.; Baboul, A. G.; Stefanov, B. B.; Liu, G.; Liashenko, A.; Piskorz, P.; Komaromi, I.; Gomperts, R.; Martin, R. L.; Fox, D. J.; Keith, T.; Al-Laham, M. A.; Peng, C. Y.; Nanayakkara, A.; Challacombe, M.; Gill, P. M. W.; Johnson, B.; Chen, W.; Wong, M. W.; Andres, J. L.; Gonzalez, C.; Head-Gordon, M.; Replogle, E. S.; Pople, J. A. *Gaussian 98*, Revision A.9; Gaussian, Inc.: Pittsburgh, PA, 1998.

(14) Gustafson, T. L.; Chernoff, D. A.; Palmer, J. F.; Roberts, D. M. In *Time-Resolved Vibrational Spectroscopy*; Atkinson, G., Ed.; Gordon and Breach Science: New York, 1987; p 265.

(15) Hamaguchi, H.; Urano, T.; Tasumi, M. *Chem. Phys. Lett.* **1984**, *106*, 153.

(16) Meić, Z.; Güsten, H. *Spectrochim. Acta A* **1978**, *34*, 101.

(17) Myers, A. B.; Trulson, M. O.; Mathies, R. A. *J. Chem. Phys.* **1985**, *83*, 5000.